Appl. Phys. B 74 [Suppl.], S245–S251 (2002)
DOI: 10.1007/s00340-002-0892-x

Applied Physics B
Lasers and Optics

M. ZAVELANI-ROSSI[1]
D. POLLI[1]
G. CERULLO[1,✉]
S. DE SILVESTRI[1]
L. GALLMANN[2]
G. STEINMEYER[2]
U. KELLER[2]

Few-optical-cycle laser pulses by OPA: broadband chirped mirror compression and SPIDER characterization

[1] Istituto Nazionale per la Fisica della Materia, CEQSE-CNR, Dipartimento di Fisica, Politecnico, P.za L. da Vinci 32, 20133 Milano, Italy
[2] Institute of Quantum Electronics, Swiss Federal Institute of Technology, ETH Hönggerberg, HPT, 8093 Zürich, Switzerland

Received: 18 September 2001/
Revised version: 4 December 2001
Published online: 20 June 2002 •

ABSTRACT We report double-chirped mirrors with custom-tailored dispersion over a bandwidth of 170 THz in the visible. The mirrors are employed in a prism-less compressor for ultra-broadband pulses generated by a non-collinear visible optical parametric amplifier. We also report on the full characterization in amplitude and phase of the compressed pulses by the spectral phase interferometry for direct electric field reconstruction technique, extended to the visible range. The compressed pulses display an almost flat phase from 510 to 710 nm and have nearly transform-limited 5.7-fs duration. Our measurements indicate a potential to further extend the useable bandwidth of mirror-only dispersion-compensation schemes using novel chirped mirror design approaches.

PACS 42.65.Re; 42.65.Yj; 42.79.Nv

1 Introduction

Recently, several ultra-fast optical techniques have shown the capability to generate coherent light pulses with bandwidths well in excess of 100 THz, either directly from a laser oscillator [1, 2] or by extracavity spectral broadening [3, 4] and subsequent broadband amplification [5–7]. The compression of such pulses to a near transform-limited duration calls for the development of delay lines with dispersion characteristics accurately controlled over such broad bandwidths. Chirped dielectric mirrors [8, 9] are a powerful tool for dispersion control; they introduce a frequency-dependent group delay (GD) by reflecting different frequency components of the incident radiation at different positions within the multilayer structure. Chirped mirrors are often used in conjunction with other dispersive elements, such as prism or grating pairs, to achieve the desired phase characteristics; these additional elements, however, increase the complexity of the system, making it bulky and more sensitive to alignment. Chirped mirror-only dispersion compensation has the advantage of greatly simplifying the system design, allowing for compactness, reproducibility and insensitivity to misalignment, which are of great importance in real-world applications. This dispersion management strategy was previously applied to laser oscillators [10], optical parametric oscillators [11] and extracavity pulse compressors [12].

The characterization of ultra-broadband pulses with duration in the sub-10-fs regime is a crucial point. Traditional autocorrelation techniques, which require a priori knowledge of the pulse shape, provide only rough estimates of the pulse duration. An accurate pulse characterization requires a full knowledge of the amplitude and phase of the pulse. To this purpose, several methods have been proposed, among which the most popular are frequency-resolved optical gating (FROG) [13, 14] and spectral phase interferometry for direct electric field reconstruction (SPIDER) [15, 16]. These techniques have been prevalently employed with near-infrared pulses and their extension to the visible spectral range, especially with very short pulses, is not straightforward.

In this work we report the design and construction of chirped mirrors with custom-tailored dispersion characteristics over a bandwidth of 170 THz in the visible, extending from the blue (510 nm) to the red (710 nm) spectral regions. We use these mirrors in a prism-less compressor for the pulses generated by an ultra-broadband non-collinear optical parametric amplifier (OPA) [5–7, 17–22]. We perform a full characterization in amplitude and phase of the compressed OPA pulses, using the SPIDER technique, here extended to the visible spectral range for the first time. The pulses display an almost flat phase from 510 to 710 nm and have nearly transform-limited 5.7-fs duration. The prism-less compressor greatly simplifies day-to-day adjustment of the system, making it a very useful tool for ultra-fast spectroscopy with extreme time resolution [23, 24]. In addition, our measurements indicate a potential to further extend the useable bandwidth of mirror-only dispersion-compensation schemes using novel chirped mirror design approaches.

The paper is organized as follows. In Sect. 2 we describe the experimental setup of the non-collinear OPA and characterize the group delay of the ultra-broadband amplified pulses. In Sect. 3 we describe the design and realization of the double-chirped mirrors used in the compressor. In Sect. 4, after briefly reviewing the principles of SPIDER, we outline the experimental setup used for the characterization of the compressed visible pulses and present the experimental results. Finally, in Sect. 5 we draw the conclusions and discuss prospects

✉ Fax: +39-02/2399-6126, E-mail: giulio.cerullo@polimi.it

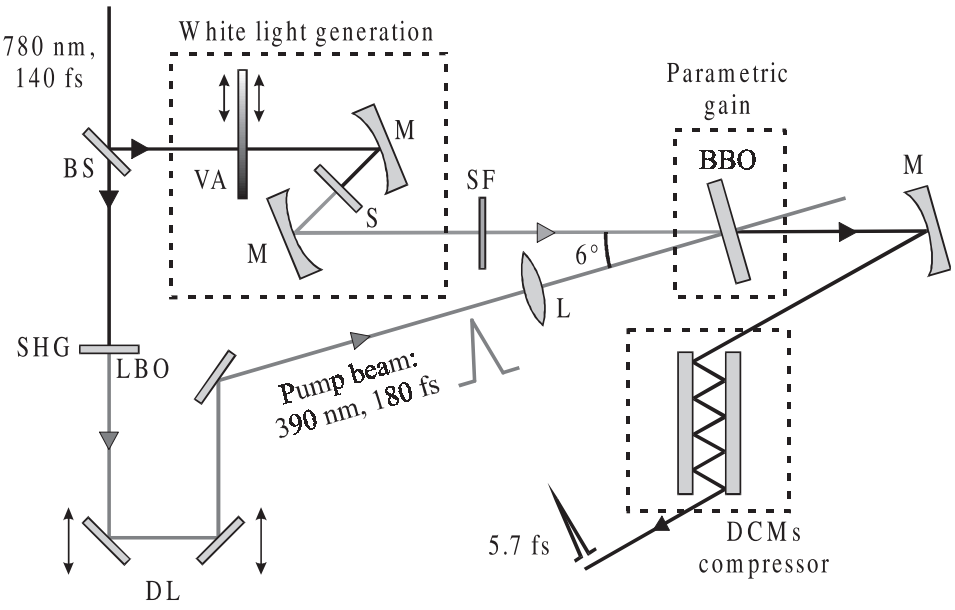

FIGURE 1 Schematic of the non-collinear OPA and the pulse compressor: BS, beam splitter; SHG, second-harmonic generator; LBO, lithium triborate crystal; DL, delay line; L, spherical lens; VA, variable attenuator; M, spherical mirrors; S, 1-mm-thick sapphire plate; SF, short-pass filter; BBO, β-barium borate crystal; DCMs, double-chirped mirrors

for increasing the bandwidth of the prism-less dispersion-compensation scheme.

2 The non-collinear ultra-broadband OPA

A schematic of the experimental setup of the non-collinear OPA used in our experiments is shown in Fig. 1 [5, 18, 20, 21]. Briefly, it starts from an amplified Ti:sapphire laser (Clark-MXR model CPA-1) producing 140-fs pulses at 780 nm and 1-kHz repetition rate with energy up to 750 μJ. The pump pulses for the OPA (390-nm wavelength, 10-μJ energy, ∼ 180-fs duration) are obtained by frequency doubling a major fraction of the light in a 1-mm-thick lithium triborate crystal. We produce the seed pulses by continuum generation obtained by focusing a small fraction (1–2 μJ) of the remaining 780-nm light beam in a 1-mm-thick sapphire plate. We use, for the plate, the minimum thickness allowing for stable white-light generation in order to minimize the GD of the seed pulse. Parametric gain is obtained in a single pass through a 1-mm-thick β-barium borate (BBO) crystal, cut at $\theta = 32°$, by use of type I phase matching, with a pump-seed angle of 3.7°, which provides the broadest gain bandwidth for the non-collinear interaction [25]. Pump intensities of $\approx 120\,\mathrm{GW/cm^2}$ are used; at higher intensities distortion and beam breakup due to higher-order non-linear effects in the BBO crystal are observed. The amplified pulses have ∼ 2 μJ energy, a peak-to-peak fluctuation of less than 7%, $\mathrm{TEM_{00}}$ beam quality and a 1-kHz repetition rate. The white-light seed and the amplified beam are guided by reflective optics only to avoid the introduction of additional chirp.

Optimum alignment is achieved by adjusting the pump-seed angle to match the apex angle of the strong superfluorescence cone emitted by the BBO crystal [26]; under these conditions, the spectrum of the amplified beam spans the whole bandwidth of the parametric process in BBO, extending from 500 to 750 nm (dashed line in Fig. 2). For reasons to be discussed later, in the experiments here reported we suppressed part of the non-collinear OPA spectrum on the low-frequency side by inserting a thin short-pass glass filter into the seed-beam path. A typical spectrum thus obtained is shown in Fig. 2 as a continuous line.

The pulses emerging from the OPA are strongly chirped; before designing the compressor, we first carefully characterized their GD. The experimental setup of the apparatus we used is shown in Fig. 3. An interference filter with 10-nm bandwidth selects a spectral slice of part of the non-collinear OPA pulses, producing ∼ 70-fs gate pulses. These pulses and the broadband OPA pulses are cross-correlated in a 20-μm-thick BBO crystal. After the crystal a UV monochromator selects the single frequencies of the up-converted signal, allowing us to determine the relative arrival times of the different frequency components of the OPA pulse. The results of

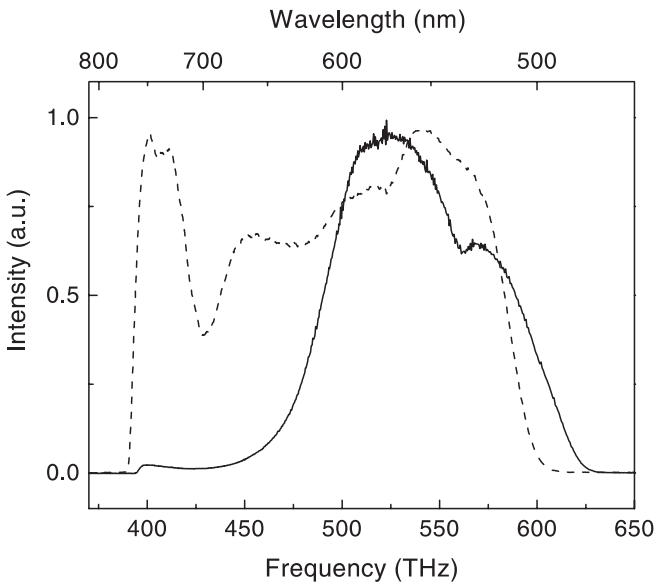

FIGURE 2 Non-collinear OPA spectrum with full-bandwidth operation (*dashed line*) and with a short-pass filter on the seed beam (*solid line*)

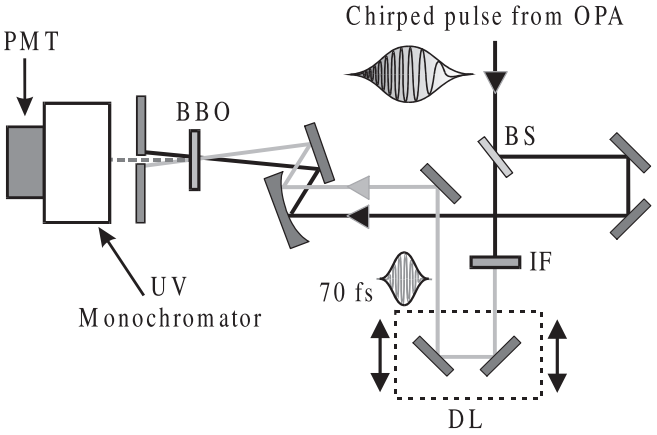

FIGURE 3 Schematic of the setup used for measuring the group delay of the amplified pulses: PMT, photomultiplier; BBO, β-barium borate crystal; BS, beam splitter; IF, interference filter (10-nm bandwidth); DL, delay line

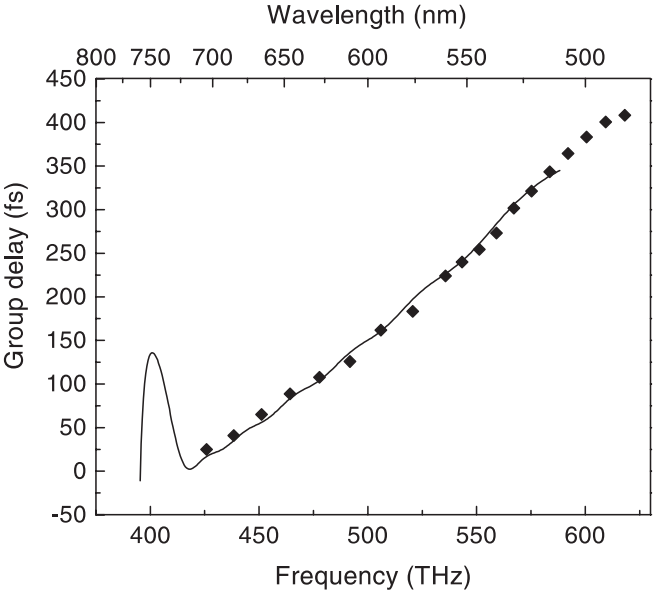

FIGURE 4 *Diamonds*, measured GD of the non-collinear OPA pulses before compression; *solid line*: GD (with reversed sign) after 10 bounces on the DCMs

the measurement are shown in Fig. 4 as diamonds: an overall group delay of ~ 400 fs between the extreme parts of the amplified pulse is measured. The experimental data can be accurately reproduced by an independent calculation of the GD. The calculation takes into account the group delays introduced by the different optical elements (sapphire plate, BBO crystal, beam splitters and air path). The measured GD vs. frequency dependence notably deviates from a linear behavior due to higher-order dispersion.

3 Pulse compression using double-chirped mirrors

Based on these measurements, we designed a prismless compressor to exactly compensate for the dispersion in Fig. 4. To achieve the required phase characteristics over ultra-broad bandwidths we used the double-chirped mirror [9, 27] approach. The simplest type of chirped mirrors is composed of alternating quarter-wave layers of high and low refractive index materials, in which the Bragg wavelength is varied from layer pair to layer pair, such that long wavelengths are made to penetrate deeper into the mirror structure than short ones. Such mirrors introduce a negative group-delay dispersion (GDD) and additionally exhibit a broader high-reflectance range compared to standard quarter-wave Bragg mirrors. The main problem in chirped mirrors is avoiding interference between reflections from the front section and the back of the mirror, which create an effective Gires–Tournois interferometer introducing large unwanted oscillations of the GD with wavelength. These dispersion oscillations can only be reduced by time-consuming computer optimization.

It has recently been shown [9] that the coupled-mode equations describing a Bragg mirror are equivalent to describing voltage and current of a microwave transmission line. In this picture any impedance discontinuity in the transmission line causes a spurious reflection, giving rise to dispersion oscillations. Adiabatic matching of the impedance is suitable for suppressing this problem. Matching is achieved by a sufficiently slow increase of the coupling coefficient in the front section of the mirror, i.e. an additional chirp in the optical thickness ratio of high-index and low-index layers. The resulting structure is called a double-chirped mirror (DCM), as it combines the chirp of the Bragg wavelength and that of the layer duty cycle. Matching within the layer stack only provides a partial solution to the problem. It has to be combined with an additional matching section to the impedance of the ambient medium on top of the DCM structure. For this purpose, an antireflection (AR) coating is typically deposited on top of the chirped mirror. This concept allows us to achieve highly controlled dispersion characteristics over bandwidths approaching 200 THz. A bandwidth limitation, however, is imposed by the broadband antireflection coating matching the coating to the ambient medium (air).

Using the DCM concept we designed mirrors with the following properties: (a) high reflectivity in the OPA wavelength range, (b) incorporation of a long-wavelength transmission window to suppress the remaining fundamental wavelength component of the seed pulse and (c) a GDD vs. frequency characteristic that allows to compensate, in a finite number of bounces, for the OPA dispersion. The main contributions to the OPA dispersion are 1 mm of sapphire, 1 mm of BBO and the air path of the setup. The chirped mirrors consist of 30 pairs of alternating SiO_2/TiO_2 layers and were manufactured by ion-beam sputtering which, together with on-line optical monitoring during the process, gives very reproducible results. We estimate a layer-deposition accuracy of ≈ 0.2 nm (rms). As shown in Fig. 5 (dashed line), the mirrors display a high reflectivity larger than 99.8% in the 480–750-nm spectral range. The designed GDD of the mirrors (solid line in Fig. 5) is negative over the 510–710-nm wavelength range and oscillates around the desired value (dotted line in Fig. 5) with an ≈ 8–9-fs^2 oscillation amplitude. In the group-delay picture, the dispersion oscillations translate into only 0.15 fs (rms) deviations from the designed value (solid line in Fig. 6). That makes it clear that such small residual dispersion oscillations, which are ultimately unavoidable even with the DCM concept and subsequent computer optimization, cause only negligible deterioration of the pulse quality. The dispersion-compensation range is further limited by the roll-on of the incorporated filter at 780 nm, which introduces phase distor-

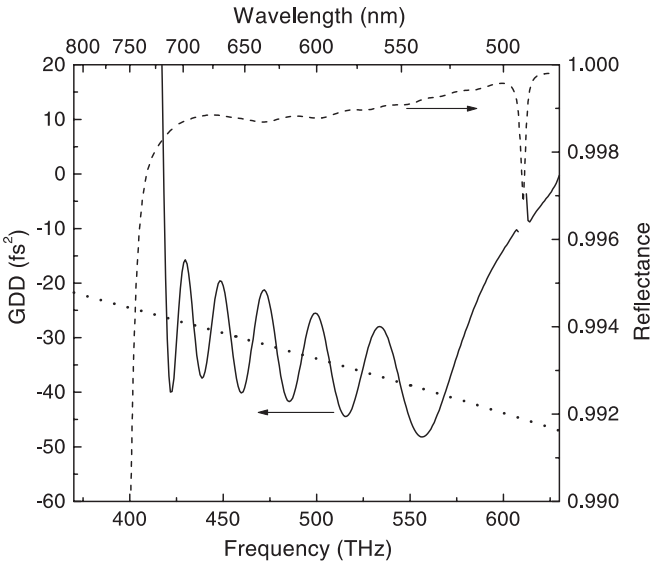

FIGURE 5 Reflectivity of the DCM (*dashed line*), designed (*solid line*) and desired (*dotted line*) GDDs of the DCM

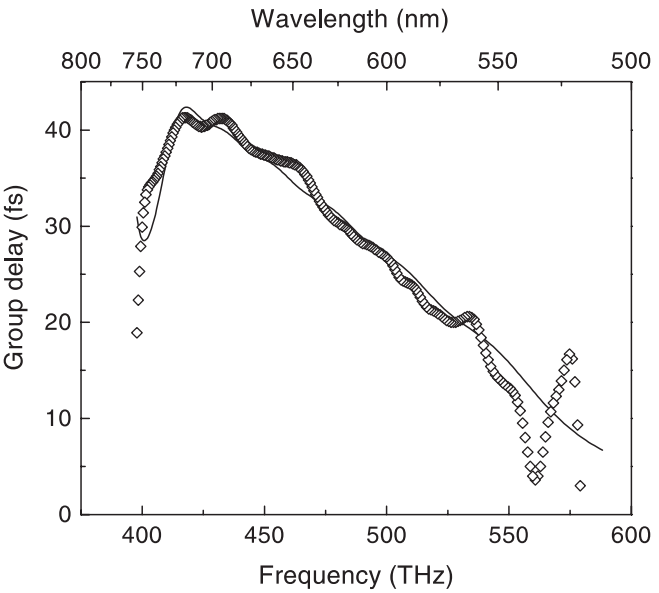

FIGURE 6 Calculated (*solid curve*) and measured (*diamonds*) group delays introduced by the DCMs

tions at above 720 nm. For this reason we are unable to compress the OPA pulse under full-bandwidth operation (dashed line in Fig. 2) and must introduce a thin colored glass filter on the seed beam to suppress part of the red spectrum in the amplified pulses.

Figure 6 shows the calculated GD of the mirrors as a solid line. We can see that the GDD oscillations are averaged out by integration and the GD displays a smooth frequency dependence with very low residual dispersion oscillations. Diamonds indicate measurements of the GD of the manufactured mirrors as measured by white-light interferometry [28]. Within the accuracy of these measurements, the experimental data fits well to the designed values. For a more illustrative image of the DCM properties, Fig. 7 shows the calculated standing wave intensity distribution inside the DCM coating. It can clearly be seen that

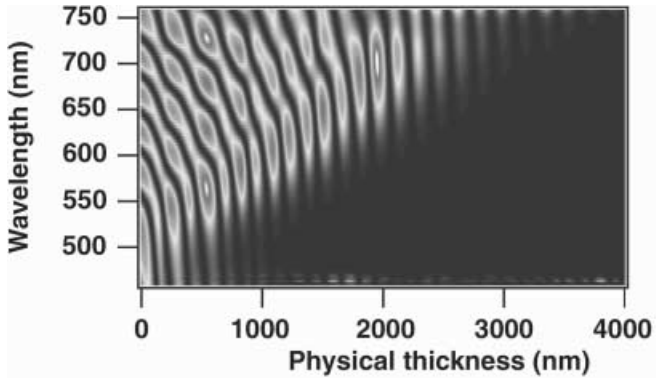

FIGURE 7 Normalized standing wave intensity distribution inside the DCM vs. wavelength. The dispersion of the mirrors is clearly illustrated by the dependence of penetration depth on wavelength

longer wavelengths penetrate deeper into the mirror structure and therefore experience a larger group delay upon reflection.

As a final check we included as a solid line in Fig. 4 the GD introduced by 10 bounces off the DCMs multiplied by −1. Again, we can see that the GD of the manufactured mirrors matches the OPA GD very accurately over the wavelength range from 510 to 710 nm, with a rms error of 1.8 fs. These DCMs allow for a compact and reproducible compressor for the OPA pulses, without any need for additional prism or grating sequences.

4 Cross-correlation SPIDER characterization of the compressed OPA pulses

To fully characterize the compressed pulses in amplitude and phase, we use the SPIDER technique [15, 16]. This technique extracts the spectral phase of the pulse from an interferogram obtained from the interference of two spectrally sheared replicas of the pulse to be characterized. Measurement of the spectral phase can be combined with measurement of a power spectrum of the fundamental. The combined spectral amplitude and phase information then gives access to the complex electric field of the optical pulse $E(\omega) = |E(\omega)| \exp\left[\mathrm{j}\phi(\omega)\right]$ in the frequency domain. An inverse Fourier transform then returns the temporal amplitude and phase of the pulse.

To retrieve the spectral phase two replicas of the pulse to be characterized are shifted in frequency by a spectral shear Ω and delayed in time by τ. The resulting spectral interference pattern they generate is

$$S(\omega) = |E(\omega)|^2 + |E(\omega+\Omega)|^2 + 2\,|E(\omega)E(\omega+\Omega)| \times \cos\left[\phi_\omega(\omega+\Omega) - \phi_\omega(\omega) + \omega\tau\right] , \quad (1)$$

where $\phi(\omega)$ is the spectral phase of the input pulse. This interferogram can be easily recorded by an integrating spectrometer. The cosine term of (1) contains all the spectral phase information we need and it is responsible for the fringes of the interferogram. The argument of the cosine can be extracted from (1) by straightforward Fourier-transform and filtering operations [29]. Note that information on the amplitudes of the interferogram is at no point required for analysis of the

data. The constant delay τ is determined by separate spectral interferometry of the two pulse replicas. After subtraction of the linear phase term $\omega\tau$, one is left with the phase difference $\phi(\omega+\Omega)-\phi(\omega)$, from which the spectral phase is extracted by integration.

The spectral shear Ω is generated by up-converting two replicas of the pulse with a strongly stretched pulse using sum-frequency generation in a non-linear optical crystal. The up-converted pulse has to be stretched such that its instantaneous frequency can be considered constant for the duration of the pulse to be measured. The interferogram is then obtained between the two up-converted pulses, which are exact, but frequency-shifted, replicas of the pulse to be characterized.

SPIDER is a self-referencing interferometric technique, i.e. there is no need for a well-characterized reference. It is an intrinsically fast technique and has been demonstrated for real-time single-shot characterization of a 10-Hz amplifier system [30] and with refresh rates as high as 20 Hz [31]. When applied to ultra-broadband pulses, SPIDER has several advantages with respect to other pulse-characterization techniques. In particular, the accuracy of spectral phase reconstruction is widely insensitive to the phase-matching bandwidth of the up-conversion crystal and the spectral responsivity of the detector, since it depends only on the fringe spacing. In addition, there is a direct, non-iterative phase-retrieval algorithm and no moving parts in the apparatus.

The extension of this technique to the visible spectral range with ultra-broadband pulses is not straightforward and requires a careful design of the setup. The SPIDER apparatus used in this work is shown in Fig. 8. We employ a novel cross-correlation variant of the SPIDER technique, that derives the reference pulse from the infrared pump laser ($\lambda = 780$ nm) rather than from the OPA pulse to be measured. This variant has the advantage of higher signal powers and a more favorable wavelength range (300–380 nm) of the SPIDER trace. A 5-cm-long SF10 glass block (GDD: 8270 fs^2) is employed as a stretcher, which results in a spectral shear of 5.22 THz between the up-converted replicas, obtained upon dividing the delay by the GDD. A balanced Michelson interferometer with 100-μm-thick Inconel-coated beam splitters is used to generate the two replicas of the non-collinear OPA pulse. These replicas are up-converted with the stretched infrared pulse in a 20-μm-thick type II BBO crystal. Type II phase matching for sum-frequency generation provides a very broad bandwidth in the ordinary axis and a considerably narrower one in the extraordinary axis. We can take advantage of these properties by orienting the narrow-band pump beam along the extraordinary axis and the broadband OPA beam along the ordinary one [32]. The up-converted pulses are detected by a spectrograph with F/3.7 F/number, using a 1200-groove/mm grating and a 25-μm entrance slit: this setup allows us to spectrally resolve the individual fringes and still cover the full bandwidth of the SPIDER interferogram. The detector was a 1024 × 256 pixel CCD array (model INSTASPEC^{TM}IV, Oriel Instruments), Peltier-cooled to −20 °C. To calibrate the apparatus we measure the linear phase term $\omega\tau$ separately by conventional spectral interferometry. To this purpose one could use simply the interferogram of the two OPA pulse replicas; however, due to the large difference in wavelength range with respect to the SPIDER trace, even small inaccuracies of the spectrometer wavelength calibration would lead to significant errors. Therefore we prefer to record the interferogram of the second harmonic (SH) of the replica pulses, which can be done with the same spectrograph adjustment used to acquire the SPIDER trace, without changing the calibration; it was however necessary to rotate the BBO crystal in order to achieve phase matching for the SH-generation process. Since the SH and the SPIDER interferograms are not completely overlapped spectrally, a very accurate calibration of the spectrometer is needed to reliably extract the linear phase term. This is achieved by measuring the wavelength of 12 spectral lines of a mercury lamp in the UV spectral region.

Figure 9 shows the SPIDER interferogram of a typical compressed non-collinear OPA pulse [33]. The time delay τ between the two pulse replicas is 271 fs. Note that the up-converted spectrum is somewhat narrower than the OPA spectrum, due to the spectral shaping induced by the finite phase-matching bandwidth of the up-conversion process. This does not cause a problem, because the SPIDER technique relies only on the fringe spacing for the reconstruction of the spectral phase and does not need the fringe-amplitude informa-

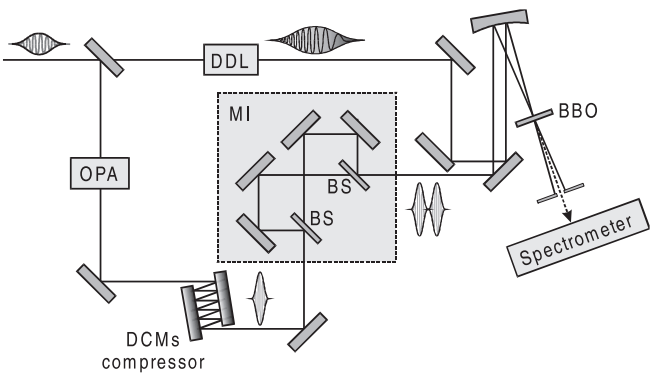

FIGURE 8 Schematic of the SPIDER setup. OPA, optical parametric amplifier; DDL, dispersive delay line; MI, balanced Michelson interferometer; BS, 100-μm-thick Inconel-coated beam splitters

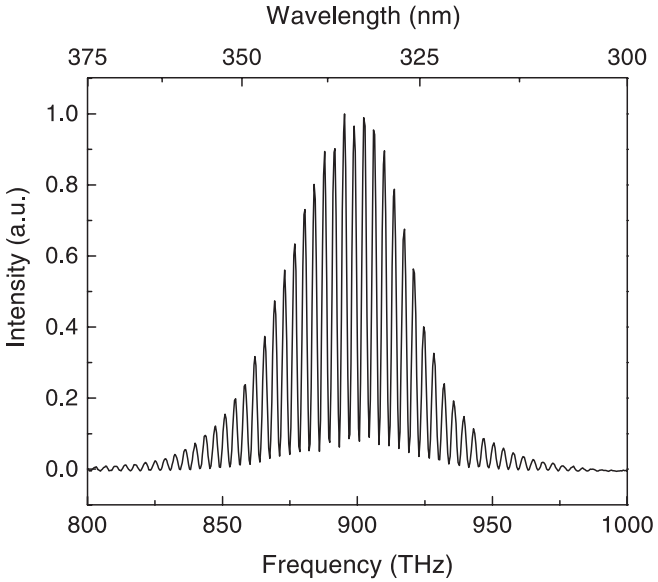

FIGURE 9 SPIDER trace of the compressed non-collinear OPA pulse

tion. The only effect of spectral shaping due to finite phase-matching bandwidth is a reduction of the signal and the consequent deterioration of the signal-to-noise ratio. In our case, however, the signal-to-noise ratio is very high even out in the tails of the SPIDER trace, so that the phase extraction is fully reliable. Using a thinner crystal would increase the phase-matching bandwidth at the expense of a lower signal, so that the thickness used in this work represents an optimum tradeoff.

The spectral phase reconstructed from the SPIDER trace is plotted in Fig. 10a (dashed line) together with an independently measured pulse spectrum (solid line). The measurements indicate a nearly flat spectral phase in the range from 510 to 710 nm. There are some residual dispersion oscillations, which are of comparable magnitude to those introduced by the 10 bounces on the chirped mirrors (compare Fig. 6). Phase distortions occur in the red for wavelengths longer than 720 nm and in the blue around 500 nm, again in agreement with the GD characteristics of the chirped mirrors. Figure 10b shows the reconstructed pulse temporal phase (dashed line) and amplitude (solid line) profile. The FWHM duration of the pulse is 5.7 fs, which is to be compared to the transform limit of 5.2 fs. The pulse shape is remarkably clean, and nearly free of side lobes. It is also confirmed that the dispersion oscillations of our DCMs have negligible impact on the pulse shape. Figure 11 shows the Wigner representation [34, 35] of the reconstructed pulse. The Wigner trace is a two-dimensional distribution in the time–frequency domain, taking into account both temporal and spectral properties of light pulses and providing an intuitive representation of the temporal ordering of the different spectral components of the pulses. It is worth noting that all the frequency components of the compressed pulses arrive simultaneously, denoting very small phase distortions of the pulse. The SPIDER measurements allow us to identify residual detrimental contributions to the spectral phase. This clearly demonstrates the advantage of using a full characterization technique over the traditional autocorrelation.

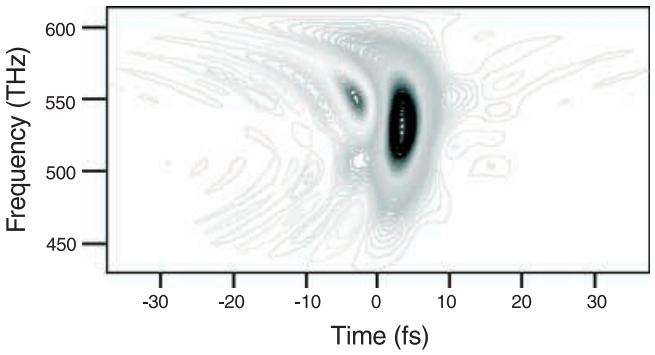

FIGURE 11 Wigner representation of the compressed OPA pulses in the time–frequency phase space

5 Conclusions and perspectives

In this work we have demonstrated the possibility of engineering DCMs with custom-tailored dispersion characteristics over bandwidths of 170 THz in the visible; these mirrors are used in a prism-less dispersive delay line to compress pulses from a non-collinear visible OPA to a near transform-limited duration of 5.7 fs. We have performed a complete characterization in amplitude and phase of the compressed pulses, revealing a nearly satellite-free pulse shape with flat spectral phase over the wavelength range 510–710 nm. Such short pulses are easily reproducible on a daily basis without any need of compressor adjustment. The DCM compressor therefore considerably simplifies the use of the OPA for spectroscopy experiments with extreme time resolution over ultra-broad bandwidths. The energy levels achievable from the OPA described in this work are sufficient for most spectroscopic applications. However, for other nonlinear optics experiments, it would be interesting to scale the output energy to the 10–100-μJ level; this could be achieved by using a multistage setup.

Our measurements indicate that, despite these results, the bandwidth of the OPA process is not yet fully exploited. The amplified spectrum obtained without any spectral filtering

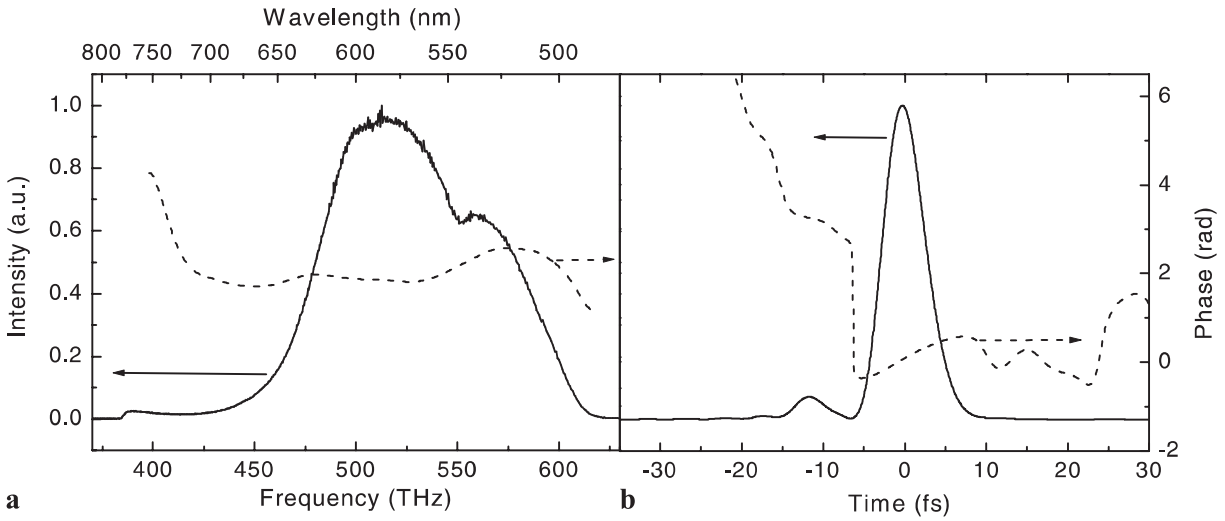

FIGURE 10 **a** Spectral intensity (*solid curve*) and reconstructed spectral phase (*dashed curve*) of the compressed non-collinear OPA pulse. **b** Reconstructed temporal intensity (*solid curve*) and phase (*dashed curve*) of the pulse

on the white-light seed, depicted in Fig. 2 as a dashed line, corresponds to a transform-limited pulse duration of 4.2 fs; such a broad bandwidth goes beyond the capabilities of the DCMs used in this work, which introduce large phase distortions for wavelengths longer than 720 nm. Two strategies can be pursued to extend the mirror bandwidth. A first limitation arises from the seed-rejection filter at 780 nm, which is incorporated in the mirror design; removing it and performing the filtering by other means would substantially alleviate constraints on the mirror design and result in a wider bandwidth. Even in this case, however, the ultimate bandwidth limitation in the DCM design is given by the impedance-matching AR coating in front of the mirror and its removal calls for a different mirror design. A novel chirped mirror concept that solves this problem was recently introduced and termed back-side coating (BASIC, [36]): here the mirror coating is deposited on the back, instead than on the front, of a thin wedged glass substrate. By choosing the substrate refractive index equal to that of the low- or high-index material of the coating, perfect impedance matching between the coating and the ambient is achieved. This mirror design allows us to achieve extremely smooth dispersion characteristics over bandwidths on the order of one optical octave. The BASIC concept, therefore, holds promise to significantly increase the chirped mirror bandwidth and should allow for a prism-less compressor working over the entire bandwidth of the non-collinear parametric process in BBO.

REFERENCES

1 D.H. Sutter, G. Steinmeyer, L. Gallmann, N. Matuschek, F. Morier-Genoud, U. Keller, V. Scheuer, G. Angelow, T. Tschudi: Opt. Lett. **24**, 631 (1999)
2 R. Ell, U. Morgner, F.X. Kärtner, J.G. Fujimoto, E.P. Ippen, V. Scheuer, G. Angelow, T. Tschudi, M.J. Lederer, A. Boiko, B. Luther-Davies: Opt. Lett. **26**, 373 (2001)
3 A. Baltuska, Z. Wei, M.S. Pshenichnikov, D. Wiersma: Opt. Lett. **22**, 102 (1997)
4 M. Nisoli, S. De Silvestri, O. Svelto, R. Szipöcz, K. Ferencz, Ch. Spielmann, S. Sartania, F. Krausz: Opt. Lett. **22**, 252 (1997)
5 G. Cerullo, M. Nisoli, S. Stagira, S. De Silvestri: Opt. Lett. **23**, 1283 (1998)
6 A. Shirakawa, I. Sakane, T. Kobayashi: Opt. Lett. **23**, 1292 (1998)
7 A. Shirakawa, I. Sakane, M. Takasaka, T. Kobayashi: Appl. Phys. Lett. **74**, 2268 (1999)
8 R. Szipöcs, K. Ferencz, C. Spielmann, F. Krausz: Opt. Lett. **19**, 201 (1994)
9 F.X. Kärtner, N. Matuschek, T. Schibli, U. Keller, H.A. Haus, C. Heine, R. Morf, V. Scheuer, M. Tilsch, T. Tschudi: Opt. Lett. **22**, 831 (1997)
10 A. Stingl, Ch. Spielmann, F. Krausz, R. Szipocz: Opt. Lett. **19**, 204 (1994)
11 J. Hebling, E.J. Mayer, J. Kuhl, R. Szipocz: Opt. Lett. **20**, 919 (1995)
12 S. Sartania, Z. Cheng, M. Lenzner, G. Tempea, C. Spielmann, F. Krausz, K. Ferencz: Opt. Lett. **22**, 522 (1997)
13 D.J. Kane, R. Trebino: IEEE J. Quantum Electron. **QE-29**, 571 (1993)
14 R. Trebino, K.W. DeLong, D.N. Fittinghoff, J. Sweetser, M.A. Krumbügel, B. Richman: Rev. Sci. Instrum. **68**, 1 (1997)
15 C. Iaconis, I.A. Walmsley: Opt. Lett. **23**, 792 (1998)
16 C. Iaconis, I.A. Walmsley: IEEE J. Quantum Electron. **QE-35**, 501 (1999)
17 T. Wilhelm, J. Piel, E. Riedle: Opt. Lett. **22**, 1494 (1997)
18 G. Cerullo, M. Nisoli, S. De Silvestri: Appl. Phys. Lett. **71**, 3616 (1997)
19 A. Shirakawa, T. Kobayashi: Appl. Phys. Lett. **72**, 147 (1998)
20 G. Cerullo, M. Nisoli, S. Stagira, S. De Silvestri, G. Tempea, F. Krausz, K. Ferencz: Opt. Lett. **24**, 1529 (1999)
21 G.<SNM>Cerullo, M. Nisoli, S. Stagira, S. De Silvestri, G. Tempea, F. Krausz, K. Ferencz: Appl. Phys. B **70**, S253 (2000)
22 T. Kobayashi, A. Shirakawa: Appl. Phys. B **70**, S239 (2000)
23 G. Cerullo, G. Lanzani, M. Muccini, C. Taliani, S. De Silvestri: Phys. Rev. Lett. **83**, 231 (1999)
24 R.A.G. Cinelli, V. Tozzini, V. Pellegrini, F. Beltram, G. Cerullo, M. Zavelani-Rossi, S. De Silvestri, M. Tyagi, M. Giacca: Phys. Rev. Lett. **86**, 3439 (2001)
25 G.M. Gale, M. Cavallari, T.J. Driscoll, F. Hache: Opt. Lett. **20**, 1562 (1995)
26 R. Danielius, A. Piskarkas, P. Di Trapani, A. Andreoni, C. Solcia, P. Foggi: Opt. Lett. **21**, 973 (1996)
27 N. Matuschek, F.X. Kärtner, U. Keller: IEEE J. Quantum Electron. **QE-35**, 129 (1999)
28 K. Naganuma, K. Mogi, H. Yamada: Opt. Lett. **15**, 393 (1990)
29 M. Takeda, H. Ina, S. Kobayashi: J. Opt. Soc. Am. **72**, 156 (1982)
30 C. Dorrer, B. de Beauvoir, C. Le Blanc, P. Rousseau, J.-P. Rousseau, S. Ranc, J.-P. Chambaret, F. Salin: Opt. Lett. **24**, 1644 (1999)
31 T.M. Shuman, M.E. Anderson, J. Bromage, C. Iaconis, L. Waxer, I.A. Walmsley: Opt. Express **5**, 134 (1999)
32 L. Gallmann, D.H. Sutter, N. Matuschek, G. Steinmeyer, U. Keller, C. Iaconis, I.A. Walmsley: Opt. Lett. **24**, 1314 (1999)
33 M. Zavelani-Rossi, G. Cerullo, S. De Silvestri, L. Gallmann, N. Matuschek, G. Steinmeyer, U. Keller, G. Angelow, V. Scheuer, T. Tschudi: Opt. Lett. **26**, 1155 (2001)
34 J. Paye: IEEE J. Quantum Electron. **QE-28**, 2262 (1992)
35 S. Yeremenko, A. Baltuška, M.S. Pshenichnikov, D.A. Wiersma: Appl. Phys. B **70**, S109 (2000)
36 N. Matuschek, L. Gallmann, D.H. Sutter, G. Steinmeyer, U. Keller: Appl. Phys. B **71**, 509 (2000)